

# Entanglement-enhanced quantum ranging in the near-Earth spacetime

Qianqian Liu<sup>1</sup>, Cuihong Wen<sup>1</sup>, Jiliang Jing<sup>1\*</sup>, and Jieci Wang<sup>1†</sup>

<sup>1</sup> *Department of Physics and Synergetic Innovation Center for Quantum Effects,*

*Key Laboratory of Low-Dimensional Quantum Structures*

*and Quantum Control of Ministry of Education,*

*Key Laboratory for Matter Microstructure and Function of Hunan Province,*

*Hunan Normal University, Changsha 410081, China*

## Abstract

We propose a quantum ranging protocol to determine the distance between an observer and a target at the line of sight in the curved spacetime of the Earth. Different from a quantum illumination scheme, here we employ a multiple quantum hypothesis testing to determine the existence and the location of the target at the same time. In the proposed protocol, the gravitational effect of the Earth influences the propagation of photons, and therefore has an observable impact on the performance of quantum ranging tasks. It is shown that the maximum potential advantages of the quantum ranging strategy in the curved spacetime has distinct superiority over its counterpart in the flat spacetime. This is because the effect of the gravitational red-shift and blue-shift on the entangled signal beam can cancel each other, while the thermal signal only suffers from the gravitational blue-shift effect. It is shown that increasing the number of transmitted modes can promote the maximum potential advantage of quantum ranging in the curved spacetime. However, the maximum potential advantage of quantum ranging in the curved spacetime can not be raised sharply by dividing the range into multiple slices.

---

\* Email: jljing@hunnu.edu.cn

† Email: jcwang@hunnu.edu.cn

## I. INTRODUCTION

Quantum illumination (QI) [1–6] is an entanglement-assisted target detection scheme where optimum quantum receivers are employed to achieve a promising advantage in error exponent against the optimal classical scenario. In addition, the employment of entanglement can solve the disadvantage of the rapid attenuation of traditional radar signals. Recently, many efforts have been put forward to make the QI schemes' theoretical advantage practically relevant [7–9] and some of these schemes have been recently experimentally demonstrated [10–12]. However, the extension of QI scheme interrogate a single spatiotemporal resolution bin at a time, restricting the real-world implementation of quantum radar [13]. Fortunately, such limitation can be resolved by a quantum-ranging protocol [14]. In such a proposal, one sends signal pulse and performs continuously measurement at the receiver side to determine the reflection of a target at line of sight [14, 15]. The main advantage of quantum ranging is the employment of the multiple quantum hypothesis testing scenario [16–18] instead of the binary hypothesis to determine the existence and the location of the target at once.

On the other hand, the novel field of relativistic quantum information aims to understand the preparation, the manipulation and the transmission of quantum information in a relativistic setting [19–32]. In particular, many experimental and theoretical proposals have been recently put forward to measure gravity induced decoherence of a quantum state [25, 26], and test the quantum nature of gravity with tabletop experiments [27, 28] based on quantum entanglement properties. Besides, quantum entanglement properties can better understand quantum clocks within relativistic settings [29], and investigate how the gravitational effect of the Earth affect satellite based quantum communication [30, 31] and clock synchronization [32] tasks. It is widely believed that the study of quantum information in a relativistic framework can provide new insights into some basic questions in quantum mechanics and relativity, such as nonlocality, causality and the information paradox of black holes. More importantly, it is of practical significance to clarify the roles of relativistic effects in realistic quantum information tasks when the parties are separated long distance in the near-Earth curved spacetime.

Quantum entanglement has been demonstrated to play a key role in the quantum ranging protocol [14]. In fact, entanglement is a kind of fragile quantum resource because noise and loss can easily destroy such a quantum resource. It is worth pointing out that the propagation pulse is affected via changing their frequency distribution in center and shape in the near-Earth curved

spacetime [30–35]. The Earth’s gravity has been found to make observable effects on the entanglement and fidelity of quantum communication [30, 31], the precision of quantum metrology [33–35], and the reliability of quantum clock synchronization [32]. Therefore, the gravitational effect of the Earth should be taken into serious consideration for practical quantum ranging tasks.

In this paper, we propose a quantum version of ranging protocol, in a more realistic scenario where the nonmaskable gravity of the Earth is considered. We are interested in how the Earth’s gravity influences the detection performance of the quantum ranging protocol. We assume that one component of the entangled signal-idler photon pair is sent from the Earth to a spatial target region to perform the quantum ranging task. The wave packet overlap and the transmissivity of the photons are deformed by the Earth’s spacetime curvature during the propagation. The maximum potential quantum advantage [36] is employed to represent the maximum possible improvement of quantum ranging protocol compared with classical ranging. It is shown that the maximum potential advantages of the quantum ranging strategy in the curved spacetime has distinct superiority over its counterpart in the flat spacetime.

The outline of the paper is as follows. In Sec. II, we outline the propagation of the photons under the background of the Earth. In Sec. III, we briefly introduce the quantum ranging tasks and calculate the potential maximum quantum advantage in different spacetime. The conclusions are drawn in Sec. IV.

## II. LIGHT WAVE PACKETS PROPAGATING IN EARTH

In this section, we consider the transmission model of light wave packets from the ground to the target region [30, 33]. The Earth’s spacetime can be approximately described by the Kerr metric, which well approximates the rotating spherical planet. For simplicity, our work will be constrained to the equatorial plane  $\theta = \frac{\pi}{2}$ . The reduced Kerr metric in the Boyer-Lindquist coordinates  $(t, r, \phi)$  is [37]

$$ds^2 = -\left(1 - \frac{2M}{r}\right)dt^2 + \frac{1}{\Delta}dr^2 + \left(r^2 + a^2 + \frac{2Ma^2}{r}\right)d\phi^2 - \frac{4Ma}{r}dt d\phi, \quad (1)$$

where  $\Delta = 1 - \frac{2M}{r} + \frac{a^2}{r^2}$ , and  $r_A, M, J$  are the radius, mass, angular momentum of the Earth, with the Kerr parameter  $a = \frac{J}{M}$ . We set  $\hbar = G = c = \kappa_B = 1$  throughout this paper.

A photon can be modeled by a wave packet of electromagnetic fields with a distribution  $F_{\Omega_K,0}^{(K)}$ , where  $K = A, B$  labels either Alice or Bob [38, 39]. Here  $\Omega_K$  and  $\Omega_{K,0}$  are the physical frequency

and the peak frequency in the corresponding transmitter. The annihilation operator for the photon is

$$\hat{a}_{\Omega_K,0}(t_K) = \int_0^{+\infty} d\Omega_K e^{-i\Omega_K t_K} F_{\Omega_K,0}^{(K)}(\Omega_K) \hat{a}_{\Omega_K}. \quad (2)$$

Such a distribution is naturally satisfied for a pulse where the optical field is described as a spatio-temporal local propagation model. The bosonic canonical commutation relations for each observer takes the form

$$[\hat{a}_{\Omega_K}, \hat{a}_{\Omega'_K}^\dagger] = \delta(\Omega_K - \Omega'_K). \quad (3)$$

Alice sends a prepared wave packet  $F_{\Omega_A,0}^{(A)}$  to the observer Bob at time  $\tau_A$ , the wave packet that propagates radially will be modified at the time  $\tau_B = \Delta\tau + \sqrt{f(r_B)/f(r_A)}\tau_A$ , where  $\Delta\tau$  represents the propagation time of the light, and  $f(r_{A(B)})$  is the gravitational frequency shifting factor at different heights. As shown in [30, 33–35, 40], we can utilize the relation between the annihilation operator  $\hat{a}_{\Omega_A}$  and  $\hat{a}_{\Omega_B}$  to obtain the relation between the frequency distributions  $F_{\Omega_K,0}^{(K)}$  before and after propagation

$$F_{\Omega_{B,0}}^{(B)}(\Omega_B) = \sqrt{\frac{f(r_B)}{f(r_A)}} F_{\Omega_{A,0}}^{(A)} \left( \sqrt{\frac{f(r_B)}{f(r_A)}} \Omega_B \right). \quad (4)$$

Compared with the observer Alice, the observer Bob has a different peak frequency and shape. These changes result from the Earth's spacetime curvature and cannot be corrected by simply shifting the frequencies linearly [38, 39]. The mode  $\bar{a}'$  received by Bob is always possible to be decomposed in terms of the mode  $\hat{a}'$  prepared by Alice and an orthogonal mode  $\hat{a}'_\perp$  [30, 33, 41]

$$\bar{a}' = \Theta \hat{a}' + \sqrt{1 - \Theta^2} \hat{a}'_\perp, \quad (5)$$

where

$$\Theta = \int_0^{+\infty} d\Omega_B F_{\Omega_{B,0}}^{(B)*}(\Omega_B) F_{\Omega_{A,0}}^{(A)}(\Omega_B), \quad (6)$$

is the wave packet overlap between the distributions  $F_{\Omega_{B,0}}^{(B)}(\Omega_B)$  and  $F_{\Omega_{A,0}}^{(A)}(\Omega_B)$ . Quality of the channel can be quantified by using fidelity  $\mathcal{F} = |\Theta|^2$ . The fidelity of photons would tend to zero when it passes through a spacetime region with strong curvature, and it would reach unity in the flat spacetime. We assume that the wave packets are Gaussian that satisfy

$$F_{\Omega_0}(\Omega) = \frac{1}{\sqrt{2\pi\sigma^2}} e^{-\frac{(\Omega-\Omega_0)^2}{4\sigma^2}}, \quad (7)$$

with wave packet width  $\sigma$ . Then we employ (6) and (7) to obtain

$$\Theta_{1(2)} = \sqrt{\frac{2(1 \pm \delta)}{1 + (1 \pm \delta)^2}} e^{-\frac{\delta^2 \Omega_{B,0}^2}{4(1+(1 \pm \delta)^2)\sigma^2}}, \quad (8)$$

where the new parameter  $\delta = \sqrt[4]{\frac{f(r_A)}{f(r_B)}} - 1 = \sqrt{\frac{\Omega_B}{\Omega_A}} - 1$  and signs  $\pm$  occur for the upwards (i.e.,  $r_B > r_A$ ) and downwards (i.e.,  $r_B < r_A$ ). The explicit expression of the frequency shift for the photon propagated between Alice and Bob is found to be [31]

$$\frac{\Omega_B}{\Omega_A} = \frac{1 + \epsilon \frac{a}{r_B} \sqrt{\frac{M}{r_B}}}{C \sqrt{1 - 3\frac{M}{r_B} + 2\epsilon \frac{a}{r_B} \sqrt{\frac{M}{r_B}}}}, \quad (9)$$

where  $C = \left[1 - \frac{2M}{r_A}(1 + 2a\omega) + \left(r_A^2 + a^2 - \frac{2Ma^2}{r_A}\right)\omega^2\right]^{-\frac{1}{2}}$  is the normalization constant, the parameter  $\omega$  denotes Earth's angular velocity at the equatorial. Here  $\epsilon = +1$  stand for direct orbits, and  $\epsilon = -1$  for the opposite way. In the Schwarzschild limit  $(a, \omega) \rightarrow (0, 0)$ , the frequency shift simplifies to

$$\frac{\Omega_B}{\Omega_A} = \sqrt{\frac{1 - \frac{2M}{r_A}}{1 - \frac{3M}{r_B}}}. \quad (10)$$

Then we get the perturbation expression of  $\delta$

$$\begin{aligned} \delta &= \delta_{Sch} + \delta_{rot} + \delta_h \\ &= \frac{1}{8} \frac{r_S}{r_A} \left( \frac{r_A - 2R}{r_A + R} \right) - \frac{(r_A \omega)^2}{4} - \frac{(r_A \omega)^2}{4} \left( \frac{3}{4} \frac{r_S}{r_A} - \frac{2r_S a}{\omega r_A^3} \right), \end{aligned} \quad (11)$$

where the parameter  $R = r_B - r_A$  is the height difference between Bob and Alice, the Schwarzschild radius of the Earth reads  $r_S = 2M$ . In addition,  $\delta_{Sch}$ ,  $\delta_{rot}$  and  $\delta_h$  denote the first order Schwarzschild term, the rotation term and the higher-order correction term, respectively. If the target is located at the height  $R \simeq \frac{r_A}{2}$ , the received photon frequency at this height will not experience any frequency shift.

Considering that the radius of the Earth is about  $r_A = 6378$  km, its Schwarzschild radius is about  $r_S = 9$  mm. We note that in Eq. (8) two different scenarios occur [30]. (i) If  $\frac{\delta \Omega_{B,0}}{\sigma} \leq \delta \ll 1$ , the wave packet overlap is  $\Theta \sim 1 - \mathcal{O}(\delta^2) \sim 1$ . In this case, the curvature effects are independent of the peak frequency and Gaussian bandwidth and negligible. (ii) The other case is  $\delta \ll \left(\frac{\delta \Omega_{B,0}}{\sigma}\right)^2 \ll 1$ , which occurs for typical communication where  $\Omega_{B,0} = 700$  THz and Gaussian bandwidth  $\sigma = 1$  MHz [42]. In this case, the wave packet overlap parameter is  $\Theta = 1 - \frac{\delta^2 \Omega_{B,0}^2}{8\sigma^2}$ .

The effect of gravity is much larger than the first scenario and must be considered in the photon propagation process. Accordingly, the final state and the wave packets overlap  $\Theta$  are related to the range  $R$  of the target in the present work.

### III. QUANTUM TARGET RANGING IN CURVED SPACETIME

The diagram of the proposed near-Earth quantum ranging proposal is shown Fig. (1). Unlike a QI scheme, the tasks of quantum ranging can not only determine the exist of a target, but also the distance between the observer and the target along the line of sight [14, 15]. As shown in Fig. (1), we assume that the distance can be divided into  $m \geq 2$  discrete intervals. The observer Alice on the ground, with a finite precision requirement  $\Delta$ , transmits a signal pulse  $\hat{a}_S$  to a target region and continuously collects the return photons  $\{\hat{a}_l\}_{l=1}^m$  at the receiver side to determine the distance. The return signal photon reaches the receiving side after time  $\{t_l\}_{l=1}^m = 2l\Delta/c$ . In hypothesis  $R$ , the target is located on the slice with  $R\Delta$  away from the observer, and the reflected mode  $\hat{a}_R$  arrives at the observer after time  $t_R = 2R\Delta/c$ . Then the problem of ranging can be modeled as the determination of the reflected mode  $\hat{a}_R$  among the continuously collect modes.

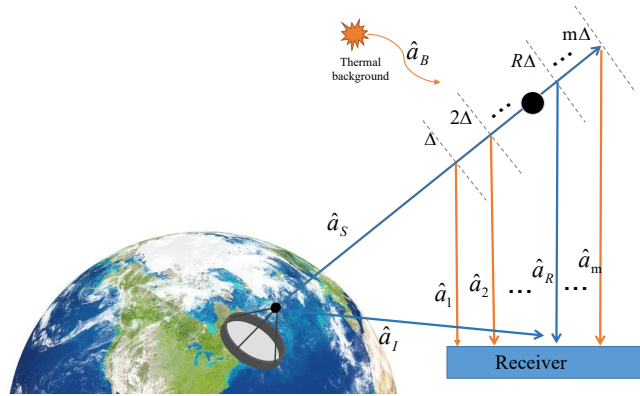


FIG. 1: (Color online) The entanglement-assisted ranging protocol under gravitational effects of the Earth. The signal and idler modes are prepared in the two mode squeezed vacuum (TMSV) state. The signal  $\hat{a}_S$  is sent out to probe the range of a target with transmissivity  $\eta$ , and the stored idler mode  $\hat{a}_I$  is correlated with the reflected signals  $\hat{a}_R$ . If the mode  $\hat{a}_R$  is detected, the target is  $R\Delta$  away from the observer.

In the present model, the Earth's spacetime curvature bring changes to the photon transmission, i.e., the frequency and shape of signal photons are affected. The reflected mode annihilation

operator at time  $t_R$  is

$$\hat{a}_R = \sqrt{\eta}\hat{a}_S + \sqrt{1-\eta}(\Theta\hat{a}_B + \sqrt{1-\Theta^2}\hat{a}_{B\perp}). \quad (12)$$

where  $\hat{a}_B$  is the thermal photon with average photon number  $N_B \gg 1$ . In the flat space limit, we have the wave packets overlap  $\Theta = 1$ , which yeilds  $\hat{a}_R = \sqrt{\eta}\hat{a}_S + \sqrt{1-\eta}\hat{a}_B$  [2, 14]. The overall transmissivity  $\eta$  can provide the ratio between received power and transmitted power [6]

$$\eta = \frac{P_R}{P_T} = \frac{GF^4 A_R \sigma}{(4\pi)^2 R^4}. \quad (13)$$

In the short range scenario, we can assume  $F = 1$  (no free space loss) and an ideal pencil beam, such that its solid angle is exactly subtended by the target's cross section  $\sigma$  [6]. This means that gain can be ideally given by  $G = \frac{4\pi R^2}{\sigma}$ . Then the overall transmissivity is found to be

$$\eta = \frac{A_R}{(4\pi R)^2}. \quad (14)$$

We can obtain a one-to-one correspondence between transmissivity  $\eta$  and range  $R$  by fixing the receive antenna collecting area  $A_R = 0.1\text{m}^2$ .

If the return signal does not reach the receiving end at time  $t_R$ , the collected photon  $\hat{a}_{l \neq R}$  is in thermal state

$$\hat{a}_{l \neq R} = \Theta\hat{a}_B + \sqrt{1-\Theta^2}\hat{a}_{B\perp}. \quad (15)$$

For the entanglement ranging protocol, we prepare an idler-signal photon pair, where one part is emitted to the space target region as the signal photon  $\hat{a}_S$ , the other part is retained in the local laboratory as the idler signal  $\hat{a}_I$ . The wave function of the TMSV state is

$$|\phi^{\text{TMSV}}\rangle_{\text{SI}} = \sum_{n=0}^{\infty} \sqrt{\frac{N_S^n}{(N_S + 1)^{n+1}}} |n\rangle_{\text{S}} |n\rangle_{\text{I}}, \quad (16)$$

where  $N_S$  is the average photon number per mode. We work on the phase space, where quantum state can be described by quadrature operators  $\hat{R} = (\hat{x}_1, \hat{p}_1, \hat{x}_2, \hat{p}_2, \dots, \hat{x}_n, \hat{p}_n)^T$ . Such operators are related to the annihilation  $\hat{a}_i$  and creation  $\hat{a}_i^\dagger$  operators by the relations  $\hat{x}_i = \frac{(\hat{a}_i + \hat{a}_i^\dagger)}{\sqrt{2}}$  and  $\hat{p}_i = \frac{(\hat{a}_i - \hat{a}_i^\dagger)}{\sqrt{2}i}$ . The quadrature operator  $\hat{R}$  satisfies the commutation relation:  $[\hat{R}_k, \hat{R}_l] = i\Omega_{k,l}$ , with  $\Omega = \bigoplus_1^{n+m} \begin{pmatrix} 0 & 1 \\ -1 & 0 \end{pmatrix}$  being symplectic form. The properties of a Gaussian state are completely specified by the first and second moment. In the phase space representation,  $|\phi^{\text{TMSV}}\rangle_{\text{SI}}$  is a zero mean Gaussian state whose corresponding covariance matrix is [43]

$$\Lambda_{\text{SI}} = \begin{pmatrix} (2N_S + 1)\mathbf{I}_2 & 2S_p\mathbf{Z}_2 \\ 2S_p\mathbf{Z}_2 & (2N_S + 1)\mathbf{I}_2 \end{pmatrix}, \quad (17)$$

where  $S_p = \sqrt{N_S(N_S + 1)}$ ,  $\mathbf{I}_2$  and  $\mathbf{Z}_2$  are the identity matrix and Pauli matrix.

For the quantum ranging protocol, we assume that the target position is on the center of the  $R\Delta$  slice. Then the overall return idle frequency state received by the receiver is [14, 15]

$$\hat{\rho}_R^E = \left( \otimes_{l \neq R} \hat{\sigma}_{\hat{a}_l}^{(B)} \right) \otimes \hat{\Xi}_{\hat{a}_R \hat{a}_I}^{(T)}, \quad (18)$$

where  $\hat{\sigma}_{\hat{a}_l}^{(B)}$  is a set of  $M$  mode thermal photon signals, and the average number of photons of each thermal photon signal is  $N_B$ . In addition,  $\hat{\Xi}_{\hat{a}_R \hat{a}_I}^{(T)}$  is the state of  $M$  mode signal-idler photon pairs returned at  $R\Delta$ , and each pair in the state is described by the covariance matrix

$$\Lambda'_{SI} = \begin{pmatrix} (1 - \Theta^2 + 2\eta N_S + \Theta^2(2N_B + 1))\mathbf{I}_2 & 2\sqrt{\eta}S_p\mathbf{Z}_2 \\ 2\sqrt{\eta}S_p\mathbf{Z}_2 & (2N_S + 1)\mathbf{I}_2 \end{pmatrix}. \quad (19)$$

In the classical strategy, the input state  $\hat{a}_S$  is assumed to have a positive P function. It is also assumed that the position of the target is on the center of the  $R\Delta$  slice. In this case the state of output signals at the receiving end is

$$\hat{\rho}_R^C = \left( \otimes_{l \neq R} \hat{\sigma}_{\hat{a}_l}^{(B)} \right) \otimes \hat{\sigma}_{\hat{a}_R}^{(T)}. \quad (20)$$

The target state  $\hat{\sigma}_{\hat{a}_R}^{(T)}$  is an  $M$  mode reflect signal embedded in a strong thermal noise background, which is generated by the thermal loss channel Eq. (12). The covariance matrix of the target state is  $[1 - \Theta^2 + \Theta^2(2N_B + 1)]\mathbf{I}_2$ .

The performance of quantum ranging strategy is measured by the bound of error probability of the hypotheses. For mixed states, it is difficult to obtain a general bound for the Helstrom limit  $P_H(\{\rho_n, p_n\})$ . An upper bound can be obtained from the pretty good measurement (PGM) [15, 44–46] described by the positive operator-valued measure

$$\Pi_n^{\text{PGM}} = \Sigma^{-1/2} p_n \rho_n \Sigma^{-1/2}, \quad 0 \leq n \leq m-1, \quad (21)$$

where  $\Sigma = \sum_{n=0}^{m-1} p_n \rho_n$ ,  $\sum_{n=0}^{m-1} \Pi_n^{\text{PGM}} = I$  and each element is positive. Therefore the error probability is

$$P_E^{\text{PGM}} = 1 - \sum_{n=0}^{m-1} p_n \text{tr}(\Pi_n^{\text{PGM}} \rho_n) \geq P_H(\{\rho_n, p_n\}). \quad (22)$$

Furthermore, the upper and lower bounds of error probability basing on the fidelity are in the form of [46, 47]

$$P_H \leq P_{H,UB} := 2 \sum_{n' > n} \sqrt{p_{n'} p_n} F(\rho_{n'}, \rho_n) \quad (23)$$



and

$$P_H \geq P_{H,LB} := \sum_{n' > n} p_{n'} p_n F^2(\rho_{n'}, \rho_n), \quad (24)$$

where  $F$  is the Bures' fidelity

$$F(\rho, \sigma) := \|\sqrt{\rho}\sqrt{\sigma}\|_1 = \text{tr} \sqrt{\sqrt{\rho}\sigma\sqrt{\rho}}. \quad (25)$$

It is assumed that each hypothesis is equal probability, that is,  $p_n = \frac{1}{m}$  for any  $n$  [15], according to symmetry  $F^2(\rho_{n'}, \rho_n) = F, \forall n \neq n'$ . Then we get the simplified boundaries

$$P_{H,UB} := (m - 1)F, \quad (26)$$

$$P_{H,LB} := \frac{m - 1}{2m} F^2. \quad (27)$$

Combining the symmetry of the whole slice range with the fidelity of the classical strategy receiving state, the lower bound of the optimal performance of the classical detection strategy can be calculated by using the positive P function input state [14]. Considering the gravitational effect of the Earth, the lower bound of classical ranging strategy is found to be

$$\begin{aligned} P'_{C,LB} &= \frac{m - 1}{2m} F^{2M}(\sigma^{(T)}, \sigma^{(B)}) \\ &\simeq \frac{m - 1}{2m} \exp \left[ -\frac{2M\eta N_S}{1 + 2\Theta^2 N_B} \right], \end{aligned} \quad (28)$$

where  $\Theta$  is the parameter of the loss channel induced by the Earth's spacetime effect given in Eq. (5).

For the quantum ranging protocol, the return signal collected at the receiver is given by Eq. (18). Because of the ranging task is symmetry, the fidelity is equal to that of discrimination between two three-mode zero mean Gaussian states. The return idler modes under two different quantum ranging hypotheses are distinguished

$$\Lambda_{12I}^{(1)'} = \begin{pmatrix} (1 - \Theta^2 + 2\eta N_S + \Theta^2(2N_B + 1))\mathbf{I}_2 & \mathbf{0} & 2\sqrt{\eta}S_p\mathbf{Z}_2 \\ \mathbf{0} & (2N_B + 1)\mathbf{I}_2 & \mathbf{0} \\ 2\sqrt{\eta}S_p\mathbf{Z}_2 & \mathbf{0} & (2N_S + 1)\mathbf{I}_2 \end{pmatrix}, \quad (29)$$

$$\Lambda_{12I}^{(2)'} = \begin{pmatrix} (2N_B + 1)\mathbf{I}_2 & \mathbf{0} & \mathbf{0} \\ \mathbf{0} & (1 - \Theta^2 + 2\eta N_S + \Theta^2(2N_B + 1))\mathbf{I}_2 & 2\sqrt{\eta}S_p\mathbf{Z}_2 \\ \mathbf{0} & 2\sqrt{\eta}S_p\mathbf{Z}_2 & (2N_S + 1)\mathbf{I}_2 \end{pmatrix}. \quad (30)$$

We can also derive lower bound [48] for the error probability of the entanglement enhanced ranging protocol in the curved spacetime

$$\begin{aligned} P'_{E,LB} &= \frac{m-1}{2m} F^{2M}(\Lambda_{12I}^{(1)'}, \Lambda_{12I}^{(2)'}) \\ &\simeq \frac{m-1}{2m} \exp\left[-\frac{2M\eta N_S}{1+\Theta^2 N_B}\right]. \end{aligned} \quad (31)$$

The corresponding bounds  $P_{C,LB}$  and  $P_{E,LB}$  in the flat space can be obtained by setting  $\Theta = 1$  in the Eqs. (28-31). In the curved spacetime, the wave packet overlap parameter  $\Theta = 1 - \frac{\delta^2 \Omega_{B,0}^2}{8\sigma^2}$  is less than 1. Therefore, we can obtain the conclusion that the spacetime effect of the Earth can reduce the error probability of the quantum ranging. This result is similar with the performance of QI in the Earth spacetime [49].

We now proceed to give a physical interpretation of this phenomenon. Here the ranging task is performed in the curved spacetime, both the signal  $\hat{a}_S$  and the thermal photon  $\hat{a}_B$  are deformed due to the gravitational effects. Differently, the entangled signal  $\hat{a}_S$  in the present model is propagated upwards and downwards before reaching the receiver. Therefore, the effect of the gravitational red-shift and blue-shift can cancel each other for the signal photons. However, the thermal signal  $\hat{a}_B$  returned from the background spacetime is affected by the gravitational blue-shift effect before reaching the receiver. When the returned signal does not reach the receiving end at time  $t_R$ , the collected photon  $\hat{a}_{l \neq R}$  is changed from  $\hat{a}_B$  to  $\Theta \hat{a}_B + \sqrt{1 - \Theta^2} \hat{a}_{B\perp}$ , which shows that the spacetime effects decrease the contribution of the thermal background to the returned signal.

We can also see that the quantum protocol outperforms the optimal classical protocol for error probability by using the bounds derived from the above calculation. In this paper, we are interested in how the spacetime effect of the Earth affect the performance of the quantum ranging tasks. We figure out the maximum potential advantage of the quantum enhanced ranging protocol in the flat space and the Earth spacetime, respectively. The maximum potential quantum advantage can be defined by the difference between the classical and quantum lower bounds [36]

$$f\text{-}\Delta P_{\max} = P_{C,LB} - P_{E,LB}, \quad (32)$$

$$c\text{-}\Delta P_{\max} = P'_{C,LB} - P'_{E,LB}. \quad (33)$$

We use the  $f\text{-}\Delta P_{\max}$  to represent the maximum potential advantage of quantum ranging protocol in the flat spacetime. Similarly,  $c\text{-}\Delta P_{\max}$  denotes the maximum potential advantage of quantum ranging protocol in the near-Earth curved spacetime. In addition, the difference  $D(\Delta P_{\max})$  between

the maximum potential quantum advantage in the curved spacetime and its flat counterpart is

$$D(\Delta P_{\max}) = (c-\Delta P_{\max}) - (f-\Delta P_{\max}). \quad (34)$$

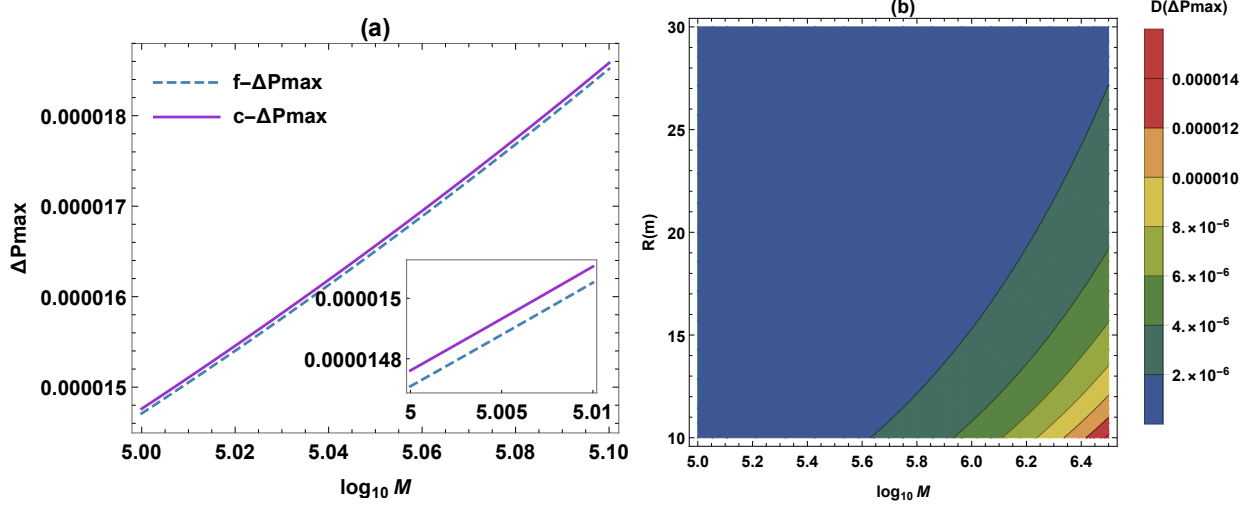


FIG. 2: (Color online) (a) The maximum potential advantage of quantum ranging strategy in the near-Earth spacetime versus the flat spacetime counterpart. The transmitter-target range is fixed as  $R = 30\text{m}$ . (b) The difference of the maximum quantum potential advantage in curved spacetime and the flat spacetime case. Here  $m = 10$ ,  $N_S = 0.01$  and  $N_B = 20$ .

Fig. 2(a) shows the maximum potential quantum advantage with respect to the number of copies  $M$  in different spacetime backgrounds. It is shown that the maximum potential advantage of quantum ranging protocol increases with the growth of the number of copies  $M$ , whether in the curved spacetime or in the flat spacetime. As we have discussed before, the maximum potential quantum advantage in the curved spacetime is higher than that of flat spacetime. In other words, the existence of gravity promotes the maximum possible advantage for the quantum ranging strategy. In Fig. 2(b), we plot the difference  $D(\Delta P_{\max})$  between the maximum potential quantum advantage in the curved spacetime and its flat counterpart. The results show that the  $D(\Delta P_{\max})$  is always positive, which indicates that the maximum potential quantum advantage in the curved spacetime is higher than its counterpart in the flat spacetime. Furthermore, the differences increase as the copies of the transmitted modes  $M$ . Then we arrive at the conclusion that increasing the copies of transmitted modes can promote the maximum potential advantage of the quantum ranging tasks.

The quantum ranging scheme divides the range between the observer and target into  $m \geq 2$  length  $\Delta$  slices, where each hypothesis corresponds to the target being in one of the slices. In Fig.

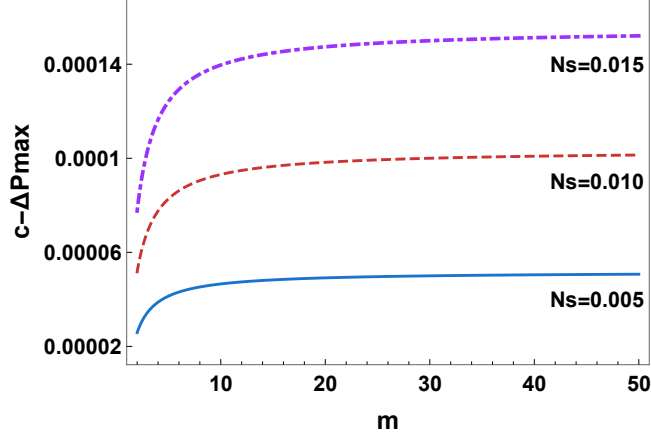


FIG. 3: (Color online) Plots of the maximum potential advantage of quantum ranging strategy in near-Earth spacetime versus the number of range slices  $m$ . The environmental thermal background noise  $N_B = 20$ , the transmitter-target range  $R = 30\text{m}$  and the number of modes  $M = 10^{5.8}$ .

2(b), we can see that the maximum potential quantum advantage in curved spacetime is superior to the flat spacetime. To gain a better understanding of the gravitational effect of Earth on the performance of quantum ranging. Fig. (3) shows the maximum potential quantum advantage in curved spacetime as a function of the number of distance slices  $m$  for different number of emitted signal photons  $N_S$ . It can be seen that the maximum potential advantage of quantum strategy increases quickly for some small number of range slices in curved spacetime. However, the  $c - \Delta p_{\text{err}}^{\text{max}}$  can not be raised sharply by dividing the range to more slices. In addition, within the value range of the number of emitted signal photons  $N_S$ , the maximum potential advantage of quantum strategy in the curved spacetime can be enhanced by increasing the emitted signal photons for  $N_S \ll 1$ . In a word, we can choose the appropriate signal energies and the number of range slices to obtain a better maximum potential advantage for the quantum ranging task in the near-Earth curved spacetime.

#### IV. CONCLUSIONS

In this paper we suggest a near-Earth quantum ranging protocol to detect the distance between the observer and the target, in which the binary quantum hypothesis in QI is replaced by the  $m$  hypothesis. In the present proposal, the performance of quantum ranging is affected by the Earth's spacetime curvature because the wave packet overlap and the overall transmissivity of the photons

are deformed by the spacetime effects during the propagation. It is shown that the maximum potential advantage of quantum strategy in the curved spacetime has distinct advantages over its counterpart in the flat spacetime. That is to say, the spacetime curvature can reduce the error probability of quantum ranging. This is because the effect of the gravitational red-shift and blue-shift on the entangled signal beam can cancel each other, while the gravity always affects the spatial return mode. What's more, we find that increasing the copies of transmitted modes can promote the maximum potential advantage of the quantum ranging tasks. The maximum potential advantage of quantum strategy increases quickly for some small number of range slices. Therefore, one can choose the appropriate signal energies and the number of range slices to obtain a better maximum potential advantage for the quantum ranging task in the near-Earth curved spacetime.

### Acknowledgments

This work is supported by the National Natural Science Foundation of China under Grant No. 12122504 and No.11875025.

- 
- [1] S. Lloyd, *Science* **321**, 1463 (2008).
  - [2] S. H. Tan *et al.*, *Phys. Rev. Lett.* **101**, 253601 (2008).
  - [3] Z. Zhang, S. Mouradian, F. N. C. Wong, and J. H. Shapiro, *Phys. Rev. Lett.* **114**, 110506 (2015)
  - [4] Q. Zhuang, Z. Zhang, and J. H. Shapiro, *Phys. Rev. A* **96**, 020302(R) (2017).
  - [5] S. Pirandola, B. R. Bardhan, T. Gehring, C. Weedbrook and S. Lloyd, *Nat. Photon.* **12**, 724-733 (2018).
  - [6] A. Karsa, G. Spedalieri, Q. Zhuang and S. Pirandola, *Phys. Rev. Res.* **2**, 023414 (2020).
  - [7] S. Guha and B. I. Erkmen, *Phys. Rev. A* **80**, 052310 (2009).
  - [8] Q. Zhuang, Z. Zhang, and J. H. Shapiro, *Phys. Rev. Lett.* **118**, 040801 (2017).
  - [9] S. Barzanjeh, S. Guha, C. Weedbrook, D. Vitali, J. H. Shapiro, and S. Pirandola, *Phys. Rev. Lett.* **114**, 080503 (2015).
  - [10] E. D. Lopaeva, I. Ruo Berchera, I. P. Degiovanni, S. Olivares, G. Brida, and M. Genovese, *Phys. Rev. Lett.* **110**, 153603 (2013).
  - [11] S. Sofer, E. Strizhevsky, A. Schori, K. Tamasaku, and S. Shwartz, *Phys. Rev. X* **9**, 031033 (2019).

- [12] F. Xu, X. Zhang, L. Xu, T. Jiang, M. Yung and L. Zhang, *Phys. Rev. Lett.* **127**, 040504 (2021).
- [13] M. Krelina, *EPJ quantum Technol.* **8**, 24 (2021)
- [14] Q. Zhuang, *Phys. Rev. Lett.* **126**, 240501 (2021).
- [15] Q. Zhuang and S. Pirandola, *Commun. Phys.* **3**, 103 (2020).
- [16] C. W. Helstrom, *J. of Stat. Phys* **1**, 231 (1969).
- [17] A. Chefles, *Contemp. Phys.* **41**, 401 (2000).
- [18] S. M. Barnett and S. Croke, *Adv. Opt. Photon.* **1**, 238 (2009).
- [19] I. Fuentes, and R. B. Mann, *Phys. Rev. Lett.* **95**, 120404 (2005).
- [20] T. G. Downes, I. Fuentes, and T. C. Ralph, *Phys. Rev. Lett.* **106**, 210502 (2011).
- [21] E. Martín-Martínez, I. Fuentes, and R. B. Mann, *Phys. Rev. Lett.* **107**, 131301 (2011).
- [22] N. Friis *et al.*, *Phys. Rev. Lett.* **110**, 113602 (2013).
- [23] J. Wang, H. Cao, J. Jing, and H. Fan, *Phys. Rev. D* **93**, 125011 (2016).
- [24] J. Wang, C. Wen, S. Chen and J. Jing, *Phys. Lett. B* **800**, 135109 (2020).
- [25] A. Bassi, A. Großardt, and H. Ulbricht, *Classical Quant. Grav.* **34**, 193002 (2017).
- [26] R. Howl, R. Penrose, and I. Fuentes, *New J. Phys.* **21**, 043047 (2019).
- [27] D. Carney, P. C. E. Stamp, and J. M. Taylor, *Classical Quant. Grav.* **36**, 034001 (2019).
- [28] G. M. Tino, *Quantum Sci. Technol.* **6**, 024014 (2021).
- [29] A. R. H. Smith and M. Ahmadi, *Nat. Commun.* **11**, 5360 (2020).
- [30] D. E. Bruschi, T. C. Ralph, I. Fuentes, T. Jennewein, and M. Razavi, *Phys. Rev. D* **90**, 045041 (2014).
- [31] J. Kohlrus, D. E. Bruschi, J. Louko, and I. Fuentes, *EPJ Quantum Technol.* **4**, 7 (2017).
- [32] J. Wang, Z. Tian, J. Jing and H. Fan, *Phys. Rev. D* **93**, 065008 (2016).
- [33] D. E. Bruschi, A. Datta, R. Ursin, T. C. Ralph, and I. Fuentes, *Phys. Rev. D* **90**, 124001 (2014).
- [34] J. Kohlrus, D. E. Bruschi, and I. Fuentes, *Phys. Rev. A* **99**, 032350 (2019).
- [35] S. P. Kish and T. C. Ralph, *Phys. Rev. D* **99**, 124015 (2019).
- [36] C. Harney, L. Banchi, and S. Pirandola, *Phys. Rev. A* **103**, 052406 (2021).
- [37] M. Visser, arXiv:0706.0622 (2007).
- [38] T. G. Downes, T. C. Ralph, and N. Walk, *Phys. Rev. A* **87**, 012327 (2013).
- [39] U. Leonhardt, *Meas. Sci. Technol.* **11**, 1827 (2000).
- [40] T. Liu, J. Jing, and J. Wang, *Adv. Quantum Technol.* **1**, 1800072 (2018).
- [41] P. P. Rohde, W. Mauerer, and C. Silberhorn, *New J. Phys.* **9**, 91 (2007).
- [42] D. Matsukevich, P. Maunz, D. Moehring, S. Olmschenk, and C. Monroe, *Phys. Rev. Lett.* **100**, 150404

(2008).

- [43] C. Weedbrook, S. Pirandola, R. G. Patrón, N. J. Cerf, T. C. Ralph, J. H. Shapiro, and S. Lloyd, *Rev. Mod. Phys.* **84**, 621 (2012).
- [44] P. Hausladen and W. K. Wootters, *J. Mod. Opt.* **41**, 2385 (1994).
- [45] P. Hausladen, R. Jozsa, B. Schumacher, M. Westmoreland, and W. K. Wootters, *Phys. Rev. A* **54**, 1869 (1996).
- [46] Q. Zhuang and S. Pirandola, *Phys. Rev. Lett.* **125**, 080505 (2020).
- [47] C. Harney and S. Pirandola, *Phys. Rev. A* **104**, 032402 (2021).
- [48] L. Banchi, S. L. Braunstein, and S. Pirandola, *Phys. Rev. Lett.* **115**, 260501 (2015).
- [49] Q. Liu, C. Wen, Z. Tian, J. Jing and J. Wang, arXiv:2104.02314